Chapter 7

# Microporous and Mesoporous Materials in Decontamination of Water Process

Rafael Alberto Fonseca-Correa,
Yesid Sneider Murillo-Acevedo,
Liliana Giraldo-Gutiérrez and
Juan Carlos Moreno-Piraján

Additional information is available at the end of the chapter

http://dx.doi.org/10.5772/64393

**Abstract**

Water pollution is the main threat that confronts humanity today. The daily human activity introduces different pollutants in hydric sources that modify water quality. This represents a high production of water that is not appropriate for different applications like human consumption. Among the water pollutants more common are dyes, herbicides, pesticides, alkanes, halo alkanes, aliphatic compounds, alcohols, carboxylic acids, aromatic compounds, detergents, surfactants, inorganic compounds (heavy metals), harmful gases, and pathogenic bacteria (bacteria and virus). These pollutants can be found in underground and surface water, and therefore can produce adverse effects on the environment and human health. These effluents can be treated with different procedures such as biological and chemical treatments, among others. However, in some cases, these processes are not appropriate for compliance legislation. Thus, adsorption with special materials such as carbon aerogels and advance oxidation processes such as photocatalysis are widely studied nowadays.

**Keywords:** aerogels, supercritical drying, SBA-15, photodegradation, photocatalysis

## 1. Introduction

The microporous materials have been used in the water decontamination process because of their adsorption capacity of a wide variety of contaminants in aqueous phase. The carbon aerogels

have become a promising material in adsorption processes of ions. The textural properties have an important function in the adsorption process. However, the adsorption treatment is not sufficient and for this reason research on new processes is necessary in water decontamination.

Within the new processes in water treatment, it has been found that the advanced oxidation process, photocatalysis, is of great importance. The photocatalyst, $TiO_2$, is used more because of its low surface area, which is a very important factor in the photocatalytic activity. For this reason, the mesoporous materials of type SBA-15 support $TiO_2$.

Therefore, the processes such as adsorption with carbon aerogels and degradation of organic compounds with Ti-SBA-15 (photocatalyst) are used for water decontamination. The textural properties of these porous materials are different but they can be complementary in processes of water decontamination.

## 2. Microporous and mesoporous materials

### 2.1. Inorganic ions adsorption on carbon aerogel

In recent years, the synthesis of nanoporous solids has received much attention, and important methods to fabricate their pore structures have been proposed recently [1–5], such as carbon aerogels. The pore continuity of aerogels, sol-gel process has attracted much attention for the fabrication of porous materials [5]. Aerogels refer to dried gels with a very high relative pore volume [6]. Pekala succeeded in the preparation of carbon aerogels, which are carbonized from organic polymer aerogels in an inert atmosphere such as nitrogen [7, 8]. Due to large surface area and easily tunable nanoporosities, these materials have potential applications in various fields, such as hydrogen fuel storage, catalysis, supercapacitors, electrodes, and anodes in rechargeable lithium ion batteries [9]. In this chapter, we show a new application of these materials to remove ions from aqueous solution, for example, nickel and chromium.

The aerogels could be divided into monolith, powder, and film; and by considering the preparation method, aerogel could be made up of four types including aerogel, xerogel, cryogel, and other aerogel-related materials, hydrogels or alcohogels. While given the different microstructure, aerogel could be classified as microporous (<2 nm) aerogel, mesoporous (2–50 nm) aerogel, and mixed-porous aerogel.

The application design of the carbon aerogel is based on its properties, which rely on the microstructure. Therefore, it is very important to realize the microstructure control during the preparation. Commonly, the preparation process of the aerogel includes the following three key steps [10], as shown in **Figure 1**:

(I–II) *Solution-sol transition*: nanoscale sol particles are formed in the precursor solution spontaneously or catalyzed by the catalysts via hydrolysis and condensation reactions.

(III–IV) *Sol-gel transition* (*gelation*): the sol particles are cross-linked and hierarchically assembled into a wet gel with the coherent network.

http://dx.doi.org/10.5772/64393

(V–VI) *Gel-carbon aerogel transition* (*drying and carbonization*): the solvent inside the wet gel was replayed by the air without serious microstructure damage and obtained the carbonaceous structure from pyrolysis.

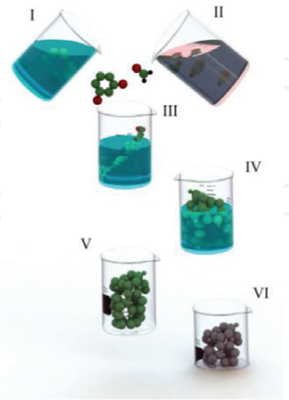


**Figure 1.** Synthesis of aerogels.

All the three steps could determine the microstructure of the aerogel and affect its properties and applications [11].

Carbon aerogel was prepared by the Pekala method via $Na_2CO_3$-catalyzed polycondensation of resorcinol with formaldehyde (RF aerogel) in an aqueous solution [12]. In fact, the random network of RF gel has been built by the homogeneous polymerization of resorcinol and formaldehyde in a large proportion of solvent (water) (**Figure 2**). The mixtures are stirred for a certain period of time and poured into cylindrical glass molds with lid.

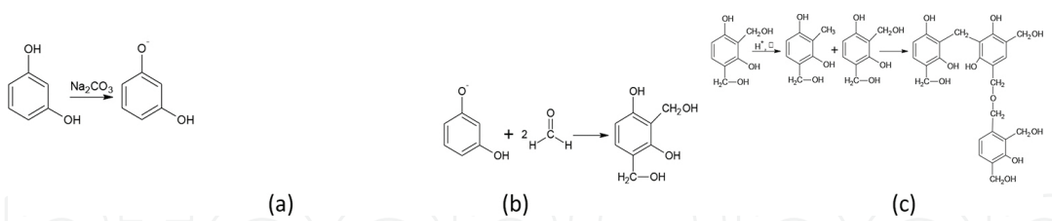


**Figure 2.** Reaction of polymerization. (a) Enolate ion formation, (b) formation of the monomer, and (c) obtaining cross-linked polymer network [12].

The resorcinol-formaldehyde wet gels were prepared using resorcinol (98% purity), formaldehyde (37% solution), $Na_2CO_3$ (99.9% purity), all from Aldrich, and deionized water. Resorcinol (0.29 mol) was dissolved in deionized water at a certain R/W ratio. Solution of formaldehyde was added to the resorcinol solution (R/F = 0.5) in vigorous stirring. Afterward, $Na_2CO_3$ in 0.1 M aqueous solution was added to the previous mixture at different ratios and R/C 100, 400, and 600 samples were obtained. The solutions were placed into tightly closed glass molds (7 cm length × 1 cm internal diameter) and cured: However, the rate of these reactions in the room temperature is very slow. Normally, a multiple-stage heating process is used to accelerate the gelation, 1 day at room temperature, 1 day at 50°C, and 3 days at 70°C.

Conventionally, the term "aerogels" has been use to designate gels dried under supercritical conditions. Supercritical drying mostly affects only the larger pores that involve network dimensions. The critical point parameters of $CO_2$, which is the most commonly used fluid, are as follows: $T_c$ (°C) 31.0, $P_c$ (bar) 74 [13]. The removal of water becomes essential in the case of supercritical drying (**Figure 3**) with $CO_2$ because of the insolubility between $CO_2$ and water, the aqueous solvent is replaced with an organic one (e.g., methanol, acetone, isopropanol, or amyl acetate) through a repetitive washing procedure. The resulting resorcinol-formaldehyde gels were washed with ethanol followed by acetone and dried with $CO_2$ in supercritical conditions (38–40°C, 120 bar) resulting in resorcinol-formaldehyde aerogels.

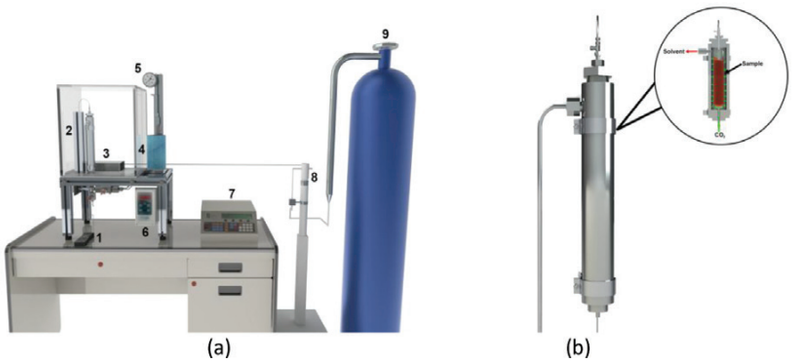


**Figure 3.** (a) Equipment for supercritical fluid used for drying the aerogels: (1) thermocouple, (2) extractor, (3) finned resistor and ventilator, (4) hot air bath, (5) condensation trap-pressure gauge, (6) temperature controller, (7) control unit of the syringe pump, (8) syringe pump, and (9) $CO_2$ cylinder and (b) extractor.

Pyrolysis of the organic polymer aerogels produces carbon aerogels, which are known to have uniform mesopores that depend on the agglomerate structures of uniform spherical carbon particles. The basic idea is to prepare carbonized RF (CRF) aerogels. The organic aerogels were pyrolyzed in $N_2$ atmosphere for 4 hours, or at 850°C samples, resulting in carbon aerogels. It is possible to obtain a CRF aerogel with ultrahigh-specific surface area by activating the carbon skeletons with carbon dioxide under high temperature (normally 800–1200°C) [14]. Carbon dioxide rather corrodes than activates the skeletons, creating more pores (mainly micropore).

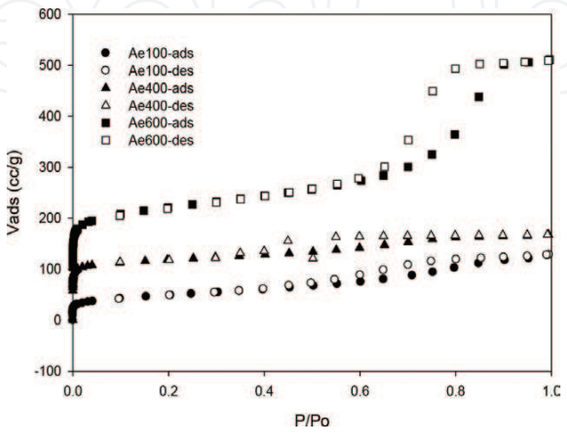


**Figure 4.** Adsorption and desorption isotherms of nitrogen on resorcinol-formaldehyde carbon aerogels at 77 K.

The aerogels are known to have outstanding characteristics (e.g., higher surface areas, total pore volumes, and sometimes electrochemical double-layer capacitances).

The structures of resorcinol-formaldehyde aerogels depend on the size and number of resorcinol-formaldehyde clusters generated during the polymerization in the synthesis process. Low-temperature nitrogen adsorption measurement is a common means for characterization of nanopore structures in materials. Adsorption and desorption isotherms of $N_2$ on the resorcinol-formaldehyde aerogels at 77 K are shown in **Figure 4**. Resorcinol-formaldehyde aerogels have type IV isotherms and a characteristic adsorption hysteresis, indicating that microporosity has had an important development regarding the mesoporosity.

The micropore and mesopore structural parameters can be determined from the $N_2$ adsorption isotherm, and in this case, the surface area of carbon resorcinol-formaldehyde aerogels was between 263 and 829 $m^2/g$, mesopore volume was between 0.16 and 0.58 $cm^3/g$, and the micropore volume was between 0.06 and 0.31 $cm^3/g$ (**Table 1**).

| Sample | *D-A* | | | | | *B-J-H* | |
|---|---|---|---|---|---|---|---|
| | $S_{BET}$ ($m^2$ $g^{-1}$) | $V_m$ ($cm^3$ $g^{-1}$) | $E_0$ (kJ $mol^{-1}$) | *n* | *L* (Å) | $V_{meso}$ ($cm^3$ $g^{-1}$) | *L* (Å) |
| **Ae100** | 263 | 0.06 | 5.97 | 2.1 | 7.7 | 0.16 | 17.1 |
| **Ae400** | 455 | 0.23 | 5.35 | 3.4 | 8.1 | 0.10 | 17.1 |
| **Ae600** | 829 | 0.31 | 8.07 | 2.2 | 7.0 | 0.58 | 39.3 |

**Table 1.** Parameter values for the low pressure range (DA) and high pressures (BJH).

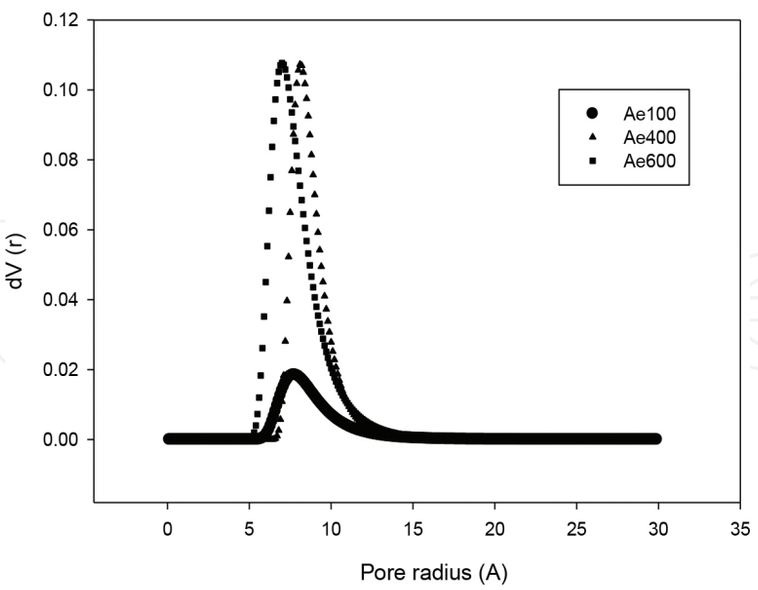


**Figure 5.** Pore size distribution D-A plot.

It means that the higher the ratio R/C increases, the Bet area increases, and hence the development of microporosity. According to the value obtained for the parameter *n* in the analysis

using the D-A method for low pressures, a marked heterogeneity is evidenced by the porosity of the aerogels. **Figure 5** shows the pore distribution obtained for the samples.

Resorcinol-formaldehyde aerogels obtained have a homogeneous distribution of micropores and mesopores, which can be seen in the SEM micrograph. **Figure 6** shows that mesopores are relatively uniformly distributed in the resorcinol-formaldehyde aerogels.

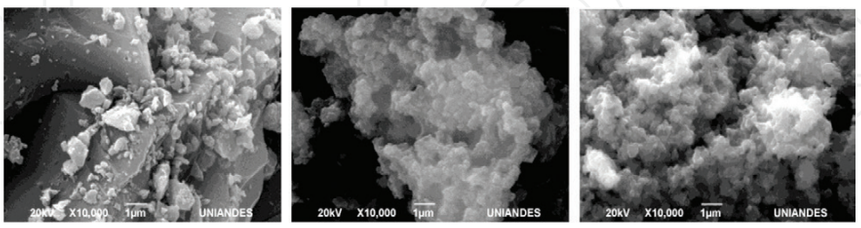


**Figure 6.** SEM image of resorcinol-formaldehyde aerogels: (a) R/C 100, (b) R/C 400, and (c) R/C 600.

The solution chemistry, pyrolysis temperature, and aerogel density affect the pore structures of carbon aerogels, and the ratio R/C also affects the chemical structure and the distribution of the groups in the surface of the aerogels.

A study to determine the effect of initial pH on the distribution of different groups onto the surface was conducted. This was performed by measuring the initial pH of synthesis as soon as all the reagents were mixed and polymerization was initiated. In addition, the pH point of zero charge ($pH_{pzc}$) was determined. Quantities of the aerogels weighed in a range from 0.050 to 0.300 g in about six samples in an interval of approximately 0.05 g, and each of the materials was placed in vials of 15 mL, and 10 mL of sodium chloride solution (0.1 N NaCl) was added to each of the materials. The vials were capped and left under constant stirring at a temperature of 298 K for 48 hours. The samples are centrifuged at 3000 rpm for 15 minutes. After that the pH of each sample was measured. The pH of each sample based on its weight is plotted, and the point of zero charge is determined as the pH at which the curve tends to all the samples in suspension. Surface chemical groups were followed according to the method of Boehm [15] (**Table 2**).

| Sample | pHi synthesis | $Na_2CO_3$ (lactones) (mEq/g) | $NaHCO_3$ (carboxylics) (mEq/g) | NaOH (phenol) (mEq/g) | $NaOC_2H_5$ (carbonyls) (mEq/g) | $HCl_{(basics)}$ (mEq/g) | $pH_{pzc}$ |
|---|---|---|---|---|---|---|---|
| **Ae100** | 8.35 | 0.045 | 0.152 | 0.000 | 0.000 | 0.005 | 6.78 |
| **Ae400** | 7.16 | 0.041 | 0.217 | 0.000 | 0.000 | 0.000 | 6.75 |
| **Ae600** | 6.31 | 0.039 | 0.178 | 0.000 | 0.000 | 0.003 | 6.62 |

**Table 2.** Initial pH of synthesis with different surface groups and pHpzc carbon aerogels.

As can be seen, the initial pH of synthesis is slightly alkaline in character, which favors the formation of monomeric agglomerates (enolate ions) at the time of initiating polymerization.

http://dx.doi.org/10.5772/64393

Once aerogel resorcinol-formaldehyde is obtained, the $pH_{pzc}$ is near neutrality, thereby inducing adsorption of cations. This variable has an effect on the adsorption capacity and allows explanation and optimization of adsorption, and this is consistent with the presence of surface groups consisting predominantly of lactones and carboxylic groups. This is very important when applying these materials to the adsorption of metal ions from aqueous solution.

The pollution of water resources due to the indiscriminate disposal of heavy metals has been causing worldwide concern for the last few decades. It is well known that some metals can have toxic or harmful effects on many forms of life. Metals, which are significantly toxic to human beings and ecological environments, include chromium (Cr), copper (Cu), lead (Pb), mercury (Hg), manganese (Mn), cadmium (Cd), nickel (Ni), zinc (Zn), and iron (Fe), etc.

Moreover, the removal of metal ions from their solutions in the presence of wastewaters may be due to the adsorption on surface and pores and also to complexation by these materials. The concentrations of some of the toxic metals such as nickel and chromium are higher than the permissible discharge levels in these effluents. Therefore, it becomes necessary to remove these heavy metals from these wastewaters by an appropriate treatment before releasing them into the environment.

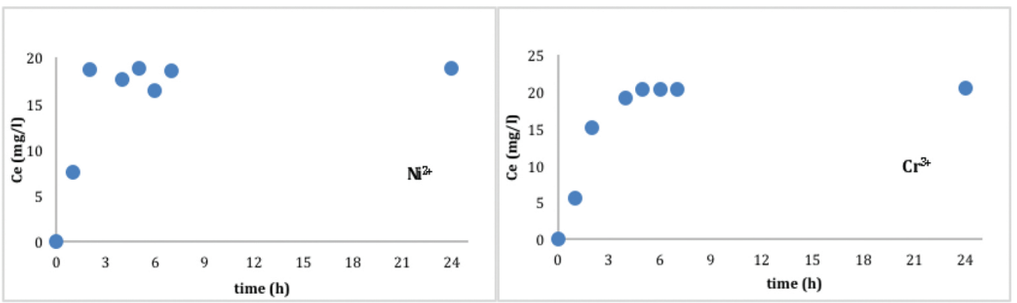


**Figure 7.** Effect of contact time on removal of $Cr^{3+}$ and $Ni^{2+}$ by carbon aerogel.

The adsorption of heavy metals such as nickel and chromium on carbon aerogel R/C 600 was studied by a batch technique. The general method used for this study is described below: A known weight of adsorbent (0.1 g) was equilibrated with 25 mL of the heavy metals solution of known concentration in a stoppered borosil glass flask at a fixed temperature in a thermostatic mechanical shaker for a known period (24 hours) of time. After equilibration, the suspension of the adsorbent was separated from the solution by filtration using Whatman No. 1 filter paper. The concentration of heavy metal ions remaining in the solution was measured by AAS using flame method. The pH of the adsorptive solutions was adjusted using nitric acid and sodium hydroxide at pH 5.0 for nickel and pH 2.0 for chromium.

It is observed that in two cases the percentage removal is comparatively lower for 3-hour contact time, with increasing removal efficiencies at higher contact time of 24 hours (**Figure 7**). It is evident from the results that the contact time required to attain equilibrium is dependent on the initial concentration of heavy metals. For the same concentration, the percentage removal of heavy metal increases with increase of contact time till equilibrium is attained. The

optimal contact time to attain equilibrium with carbon aerogel was experimentally found to be about 6 hours.

Adsorption isotherm studies were carried out with different initial $Ni^{2+}$ and $Cr^{3+}$concentrations (20–500 mg/L) and a fixed adsorbent concentration of 100 mg for 25.0 mL of solution. The equilibrium data obtained were analyzed in the light of Langmuir and Freundlich isotherms. For estimated residual metal concentration, $C_e$, the respective adsorbent metal uptake loading, $q_e$ (mg of metal per g of carbon aerogel), for each sorption system was determined using the equation

$$q_e(\text{mg/g}) = V(C_i - C_e)/W \tag{1}$$

where $C_i$ is the initial metal concentration (mg/L) in a solution of volume $V$ (L) and $W$ is the mass of adsorbent (g).

**Figure 8** shows the isotherm of nickel and chromium removal onto carbon aerogel. The following linearized forms of the Langmuir and Freundlich isotherm models were used in the present study to provide an objective framework to the generated equilibrium adsorption data. The Langmuir model allowing the calculation of maximum adsorption capacity, $Q_o$ (mg/g), and the Langmuir constant, $b$ (L/mg), is represented by the following equation:

$$C_e / q_e = 1/Q_o b + C_e / Q_o \tag{2}$$

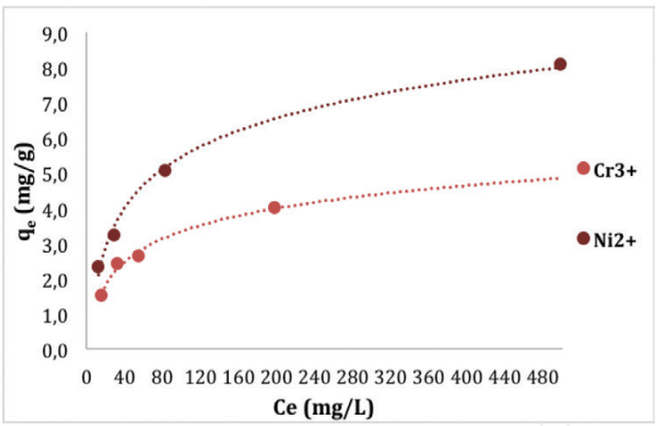


**Figure 8.** Isotherm curve for $Cr^{3+}$ and $Ni^{2+}$ adsorption onto carbon aerogel.

The linearized Freundlich model isotherm is represented by the following equation:

$$\log_{10}(q_e) = \log 10 K_f + 1/n(\log_{10} C_e) \tag{3}$$

where $K_f$ and $n$ are constants incorporating all the factors affecting the adsorption capacity and are an indication of the favorability of metal ion adsorption onto the adsorbent.

Adsorption capacity as indicated by value of "$Q_o$" is seen to be maximum for carbon aerogel, i.e., $Ni^{2+}$ 7.602 mg/g with a much lower capacities for $Cr^{3+}$. The energies of adsorption, as indicated by "*b*" are seen to be highest for $Ni^{2+}$ (**Table 3**). The values of 1/*n* lie between 1 and 10 indicating favorable adsorption.

| | Freundlich | | | Langmuir | | |
|---|---|---|---|---|---|---|
| | **KE** | **1/*n*** | ***R*²** | ***Q*ₒ (mg/g)** | ***b*** | ***R*²** |
| $Ni^{2+}$ | 11.55 | 1.265 | 0.8947 | 7.602 | 2.4125 | 0.9425 |
| $Cr^{3+}$ | 10.52 | 1.209 | 0.9089 | 4.501 | 1.9874 | 0.9117 |

**Table 3.** Values of Langmuir and Freundlich isotherm constants for the adsorption of heavy metal ions on carbon aerogel.

## 2.2. Synthesis of Ti-SBA-15 by chemical vapor deposition (CVD) like a possible photocatalyst in degradation reactions

The physical and biological treatment are not sufficient for total pollutant degradation, for this reason the heterogeneous photocatalysis is been converted into an emergent technique. This technique is nonselective and can be used in the complex samples treatment. Moreover, the sun radiation is possible to be used as a primary energy source and the oxygen as an oxidant agent. This is a clear example of sustainable technology [16].

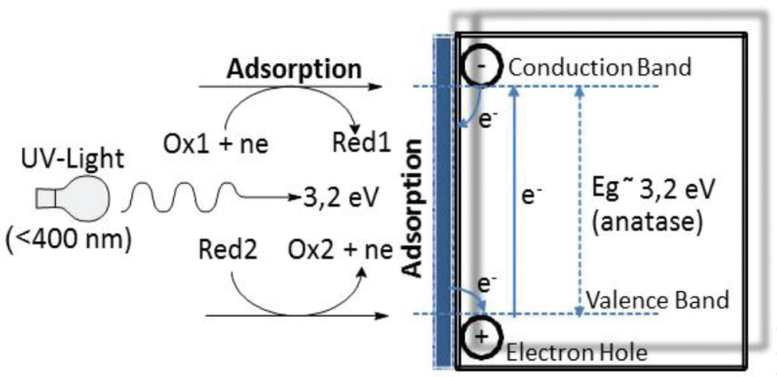


**Figure 9.** Energy band diagram $TiO_2$.

In the past decades, photocatalysis has been the research object in the contamination of water and air. The main advantages that were observed are as follows: work under environment conditions, complete destruction of pollutants and intermediaries, and low operating cost that confirmed their applicability in water treatment. However, there are many experimental and technical challenges that include (1) the commercial catalyst available presents low surface areas (factor determinant in the photocatalytic activity), (2) catalyst separation after treatment [17], (3) catalyst development with a strong absorption in the spectrum visible region [18], (4) understanding of the operation parameters of the photoreactor, and (5) mathematical inconsistencies in kinetic modeling.

In these processes, solid semiconductors are used, which are activated by UV light and $TiO_2$ (anatase), since it has a wide band-gap semiconductor (**Figure 9**) with different potential applications in catalysis, photovoltaics, optoelectronics, etc. [19, 20].

The $TiO_2$ is a good photocatalyst of organic compounds, where the absorbed light generates the formation of electron-hole pair ($e^-/h^+$). The $h^+$ interacts with the $OH^-$ ions to generate hydroxyl radicals (OH•) that have a high oxidation potential and are capable of degrading organic compounds. Electrons are trapped by oxygen to produce superoxide radicals ($O_2^-$) [21].

Charge transfer and recombination processes occur simultaneously, and the electron-hole pair is recombined before reacting with adsorbed species on the catalyst surface [22]. The efficiency of the photocatalytic reaction depends on factors that determine the degree of oxidation of organic matter. Another determining factor is the nature of the contaminant, the pH of the medium, the wavelength of the radiation, the radiation flux, and the type and concentration of oxidant [23].

Nanoparticles ($TiO_2$) can be produced in different ways, for example, chemical vapor deposition, sol-gel, the oxidation of titanium tetrachloride, and titanium alkoxides hydrolysis [24]. In addition, it is very interesting to note that to improve its photocatalytic activity and obtain spherical particles with a high surface area, it supports mesoporous materials with porous structure.

Because the $TiO_2$ has a low specific surface area (10–30 $m^2/g$) and to increase the catalytic activity, it has been chosen to be used in mesoporous materials.

## 3. Mesoporous materials

SBA-15 (Santa Barbara-15) is considered an ordered mesoporous material with hexagonal channels of diameters between 3 and 14 nm, microporous walls (0.5–2 nm), and cylinder sizes (1–3 μm) (**Figure 10**).

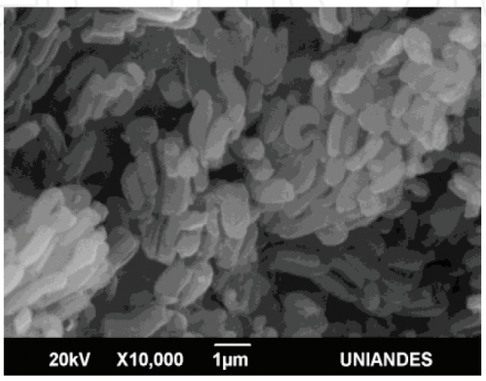


**Figure 10.** Scanning electron microscope (SEM) SBA-15.

This mesoporous solids are synthesized using triblock copolymers like a poly(ethylene oxide)-poly(propylene oxide)-poly(ethylene oxide) (PEO-PPO-PEO) $EO_{20}PO_{70}EO_{20}$ Pluronic®-123 and tetraethyl orthosilicate (TEOS) as the silicate source.

The amphiphilic will form aggregates in aqueous environment due to the PEO chains as they are hydrophilic, while the PPO chains are hydrophobic. The processes that occur in aqueous solution are: (1) the formation of micelles due to the hydrophilic groups, which are oriented to the outer of the micelles and the hydrophobic is located in the interior, and (2) solubilization of block copolymers due to the interaction between water molecules and alkylene oxides through hydrogen bonds [24, 25].

In aqueous solutions, the silicate source (TEOS) is hydrolyzed when added with water and polymerizes to form a silica network (**Figures 11–13**) [26, 27].

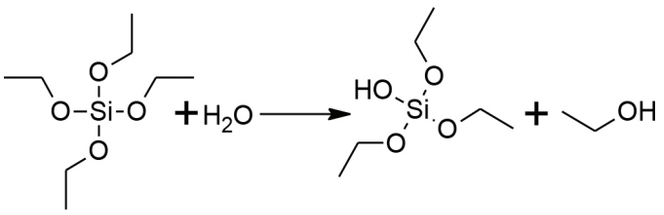


**Figure 11.** Hydrolysis of silica source.

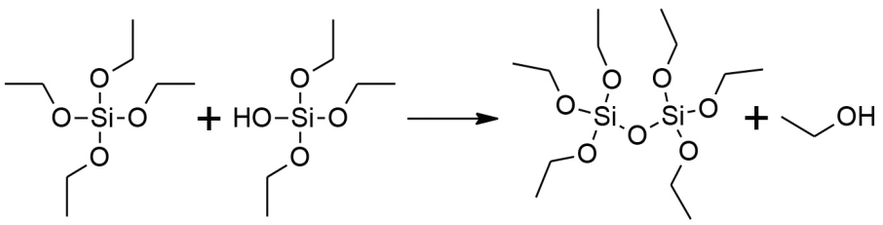


**Figure 12.** Silica network (1): alcohol condensation.

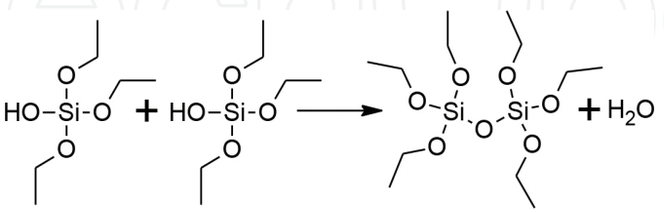


**Figure 13.** Silica network (2): water condensation.

The synthesis of SBA-15 is carried in acidic conditions because it is necessary to induce the interaction between triblock and TEOS. This can be controlled by pH in acid or basic conditions to modify the hydrolysis rate that is directly proportional to its concentration. In acidic medium, it increases the rate of hydrolysis, while in basic medium it increases the gelation

rate. For this reason, the silica source is protonated (pH < 2, since pH = 2 is the isoelectronic point) because the interactions are important at the inorganic-organic interface. In acid media, the hydronium ions are associated with the alkylene oxygen atoms; in this way the long-range Coulombic interactions are added to the coassembly process. The cationic silica is a precursor, and the mechanism is carried out through an intermediate ionic like ($S^0H^+$) ($X^-I^+$) (**Figure 14**) [28]. The silicon atom can expand the coordination sphere and allow to coordinate with the anion ($Cl^-$).

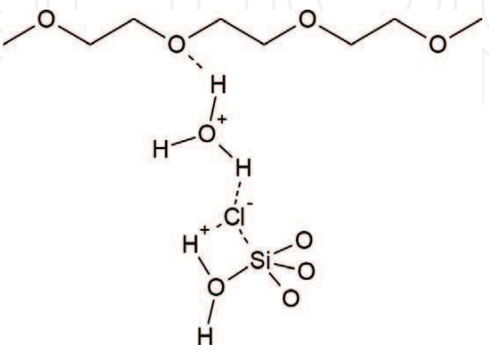


**Figure 14.** $S^0H^+X^-I^+$ interaction.

In SBA-15, the self-assembly route occurs through cooperative self-assembly, and the micellar rod cannot be formed before addition of the silica source. The micelles become elongated by the condensation of the silica source. The micellar rods arrange in a hexagonal pattern while the silica walls are built. The polymerization is simultaneous to the elongation and the silica precursor is polymerized on the PEO chains, and the water content in this area decreases to produce a change in the polarity resulting in a reduced curvature of the micelle (**Figure 15**) [29, 30].

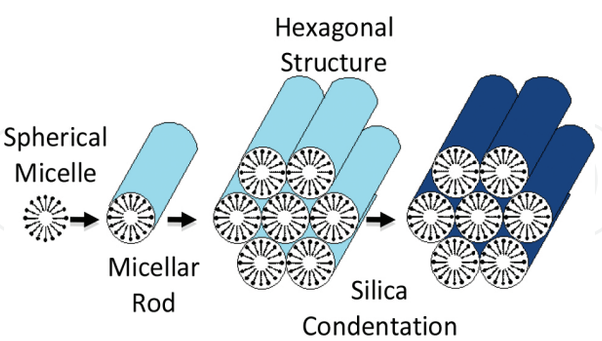


**Figure 15.** Schematic representation of SBA-15 before calcination.

The porous structures are not mesoporous (pore diameter > 2) because of the hexagonal arrangement of cylindrical aggregates. On the other hand, the PEO penetrates the pore walls, resulting in the microporous (pore diameter < 2 nm) production after calcination (**Figure 16**) [24, 25]. This process allows to remove the surfactants from SBA-15, generally the calcination temperature is 540°C for 6 hours with a rate of 5°C/min. The surfactant is decomposed between

100 and 300°C (**Figure 17**) and in this case the hexagonal structure retains its size. Above 300°C in air atmosphere, the polymers are combusted and the hexagonal framework is decreased due to its condensation. Approximately, in this stage it obtains a weight loss between 40% and 50%.

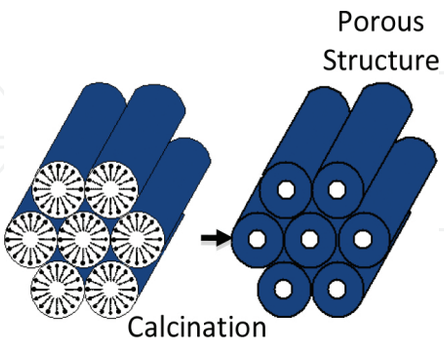


**Figure 16.** Schematic representation of SBA-15 after calcination.

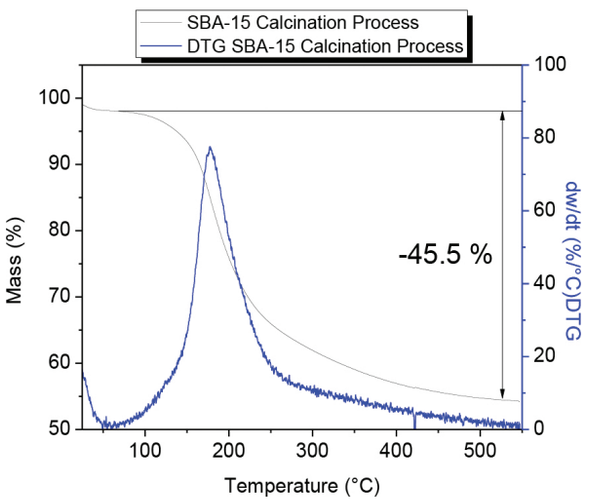


**Figure 17.** Thermogravimetric study in the elimination of surfactant.

These kinds of materials are activated with the inclusion of hetero-elements via postsynthesis or in situ methods that make them catalytically active [31, 32]. For this reason, the SBA-15 is considered one of the materials based on silica and it is considered promising because of its commercial availability, high surface area, thermal stability, and pore size distribution (PSD). On the other hand, it has been found that the addition of $TiO_2$ on these solids facilitates dispersion of anatase crystals, which are the essential active sites for degradation of contaminants and intermediaries. Ti-SBA-15 has been synthesized by chemical vapor deposition.

The CVD method for catalyst preparation has been defined as the process of deposition using reaction between surfaces sites such as OH groups and vapors of metal compounds. CVD is a useful method for the preparation of highly dispersed catalysts. The commercial $Ti/SiO_2$ catalyst was prepared by the impregnation of silica with $TiCl_4$ or an organic titanium com-

pound followed by calcination. The active catalyst contains tetrahedral $Ti^{IV}$ chemically bonded to siloxane ligands (≡SiO) [33].

In this way, the titanium is incorporated via postsynthesis. The experimental set up of CVD is depicted in (**Figure 18**). The SBA-15 is placed in a fixed-bed reactor and is first treated at 400°C in nitrogen flow, then brought back to the deposition temperature at 300°C. The nitrogen flow (150 mL/min) is saturated with $TiCl_4$ in a saturator. The saturator is immersed in a cooling bath at −10°C because of the vapor pressure of $TiCl_4$ at −10°C is 170 Pa (0.17%, V/V). The sample is then purged under nitrogen at 573 K, hydrolyzed at ambient temperature in moist air, dried at 80°C, and finally calcined in dry air at 673 K [34].

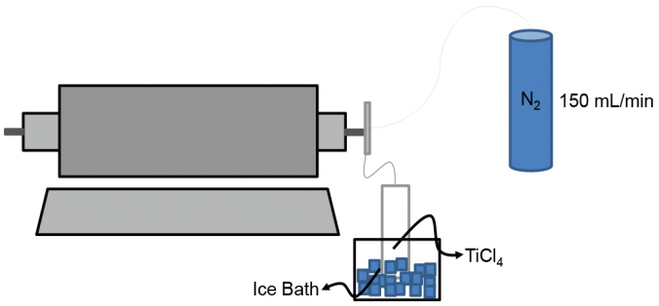


**Figure 18.** Experimental set up of chemical deposition vapor.

The reactions that can occur to the synthesized Ti-SBA-15 correspond to **Figure 19**.

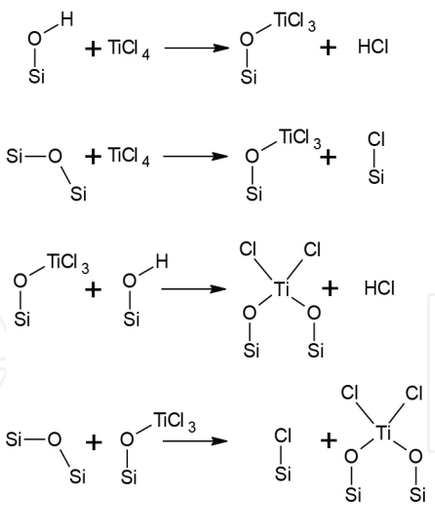


**Figure 19.** Chemical vapor deposition reaction $TiCl_4$-SBA-15.

The loss of the $OH^-$ at 3750 $cm^{-1}$ indicates that the free hydroxyl groups are reacting with the $TiCl_4$, when the deposition time is increased and the intensity of absorption peak is decreased (**Figure 20**). When a small amount of $TiCl_4$ is reacted with the silica, no change in the $OH^-$ band intensity is observed. This is observed below 8 hours of reaction. The IR absorption peaks at 1230 and 1070 $cm^{-1}$ are attributed to $\upsilon_{as}$ (Si-O-Si) vibrations of silica framework of SBA-15, and

the peak at 802 $cm^{-1}$ is attributed to υs (Si-O-Si) vibration [34]. The peak at 960 $cm^{-1}$ belongs to $v_{as}$ (Si-OH) or $v_{as}$ (Si-OH) or vas (Si-O-Ti); this peak appears by two processes:

(1) The silanol groups are reacting more quickly than the hydroxyl groups.

(2) The $TiCl_4$ starts to react with the surface; there are many sites where the surface-attached $TiCl_3$ species can react further to give a bridged $TiCl_2$ species. This gives rise to an increase in the concentration of $TiCl_3$ on the surface. When the $TiCl_3$ does not have a neighboring hydroxyl groups the reaction is completed [33].

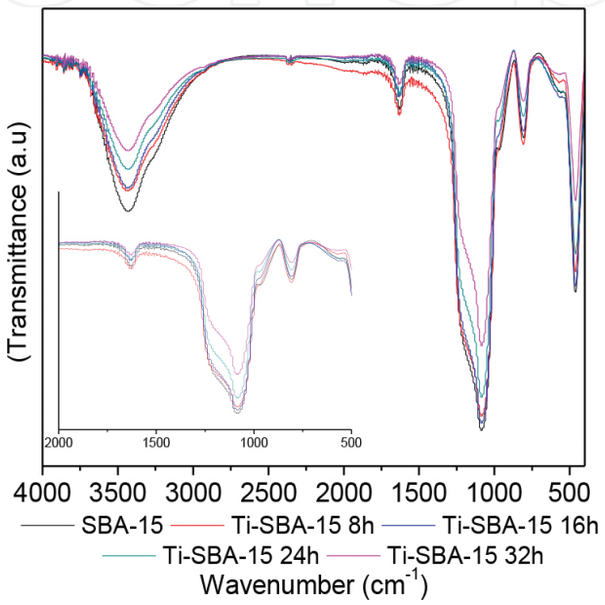


**Figure 20.** FT-IR spectra of Ti-SBA-15-h.

The relation between the peak at 960 and 802 $cm^{-1}$ can be used to evaluate the amount of the Ti-O-Si bond. As shown in **Table 4**, when an increase in the deposition time is possible, deposit more Ti species on the SBA-15 surface.

| | **(Ti/Si) = *z*** |
|---|---|
| Ti-SBA15 8h | 1.7% |
| Ti-SBA15 16h | 5.5% |
| Ti-SBA15 24h | 9.4% |
| Ti-SBA15 32h | 14.1% |

**Table 4.** Intensity ratio Ti/Si.

Textural parameters of SBA-15 and Ti-SBA-15-h are calculated from $N_2$ adsorption isotherm at 77 K (**Figure 21**) and these are presented in **Table 1**. This type of porous solid exhibited type IV isotherm and the presence of a hysteresis loop [35], which are characteristics of mesoporous

solids (2–50 nm pore size). Pore size distributions calculated with the Cylinder Pore NLDFT adsorption branch is reported in **Figure 22**. The PSD profile showed a broad peak with pore size >2 nm (mesoporous); this value corresponds at 3.4 nm to all samples.

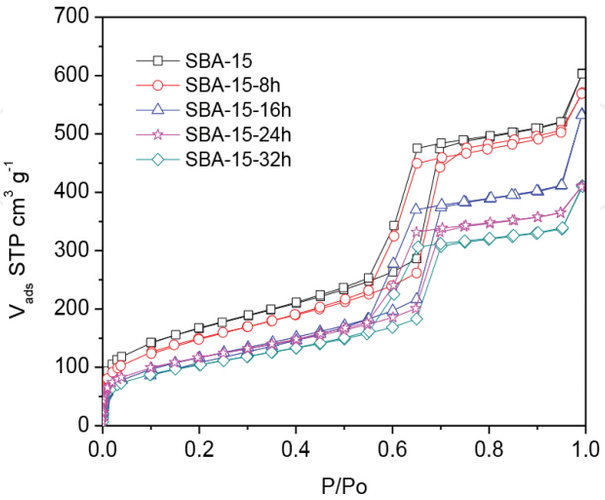


**Figure 21.** Isotherm adsorption $N_2$ 77 K.

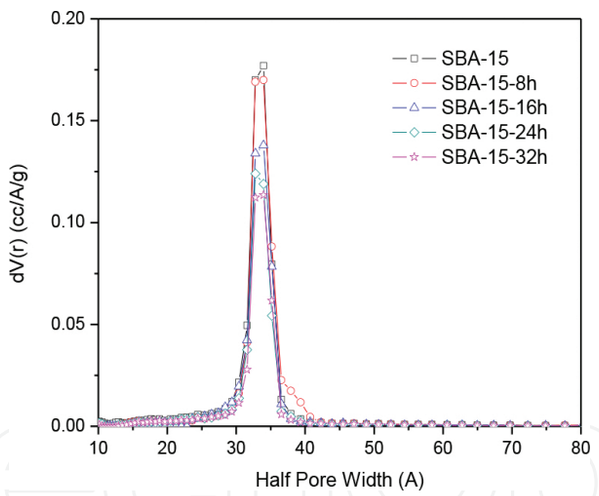


**Figure 22.** PSD obtained with $N_2$ 77 K silica (cylinder pore, NLDFT adsorption branch).

| | $S_{BET}$ ($m^2$ $g^{-1}$) | $V_{micro\ DR}$ ($cm^3$ $g^{-1}$) | $V_{meso}$ ($cm^3$ $g^{-1}$) | $V_{Total}$ ($cm^3$ $g^{-1}$) | $D_{MAX}$ (nm) |
|---|---|---|---|---|---|
| SBA-15 | 593 | 0.21 | 0.60 | 0.81 | 3.4 |
| SBA-15-8h | 537 | 0.19 | 0.59 | 0.78 | 3.4 |
| SBA-15-16h | 423 | 0.14 | 0.50 | 0.64 | 3.4 |
| SBA-15-24h | 414 | 0.15 | 0.41 | 0.56 | 3.3 |
| SBA-15-32h | 374 | 0.14 | 0.39 | 0.52 | 3.4 |

**Table 5.** Textural parameters $N_2$ adsorption data.

http://dx.doi.org/10.5772/64393

In **Table 5**, it is observed that the surface area is decreased when the deposition time is increased. The effects of CVD with $TiCl_4$ have a relation with the porosity, and the micropore volume decrease and is kept constant (0.14 $cm^3/g$) between 16 and 32 hours of deposition. The mesoporous volumes are equal for SBA-15 and Ti-SBA-15-8h, but when the deposition time is increased, the mesoporous volume decreases. This shows a similar behavior to the microporous volume. This behavior is obtained because the titanium species are supported on the surface of SBA-15. The shape of the isotherms obtained allows to deduce that there are no structural changes caused by chemical vapor deposition. Although the isotherms are parallel to the decrease in the total volume, it is due to the distribution of titanium species on the surface.

This relates to the results obtained in the IR, where Ti species on the surface increases, thereby decreasing the pore volumes. The effect of $TiCl_4$ on the surface has no effect on the textural properties.

The thermogravimetric stability was evaluated by observing that the inclusion of titanium does not affect this property because a strong interaction is developed between the titanium species and the surface (**Figure 23**). This is an important property for a photocatalyst that must be stable in a wide temperature range. The mass losses that originate are due to the calcination of the surfactant that was not removed during calcination and this allowed the porosity to be occluded (**Figure 24**).

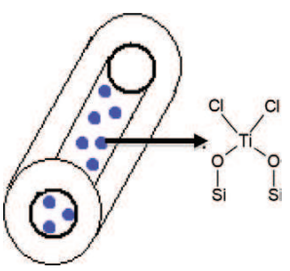


**Figure 23.** Schematic representation Ti-SBA-15-h.

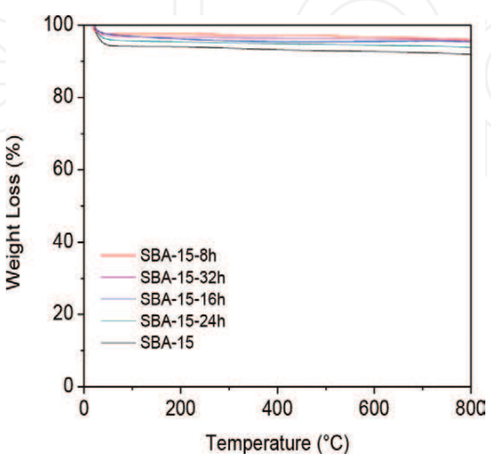


**Figure 24.** Thermogravimetric stability of Ti-SBA-15-h.

Scanning electron microscope images exhibit the morphology of SBA-15. The cylinders are the typical shape of this porous solid. The effect of chemical vapor deposition does not change the surface of the SBA morphology. The cylinders have a size of 1.4 μm and a width of 0.6 μm for all the samples (**Figure 25**). The chemical vapor deposition allows to obtain high dispersion titanium on the surface. In the SEM-EDX an increase in titanium dispersion can be observed when the deposition time is increased (**Figure 26**). These materials show a homogeneous distribution on the SBA-15 without apparent preferential concentration of titanium in some areas. The distribution is influenced for hexagonal framework of SBA-15.

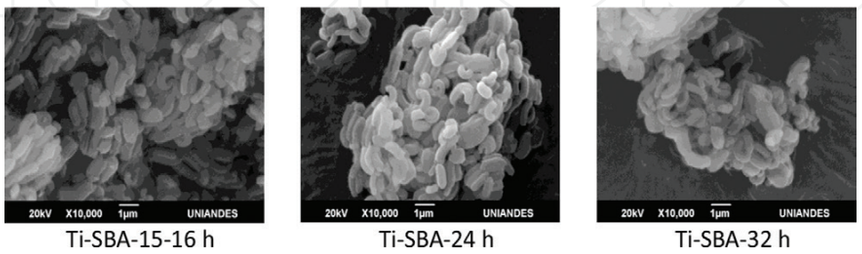


**Figure 25.** SEM of Ti-SBA-15-h at different deposition time.

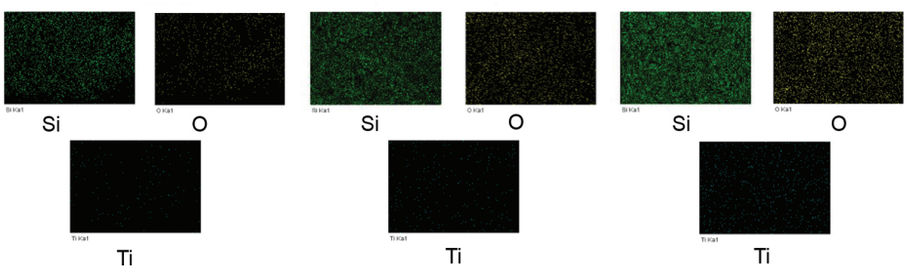


**Figure 26.** SEM-EDX dispersion titanium on the surface of SBA-15.

## 4. Conclusion

The development of new materials such as carbon aerogels for specific applications such as retention of metal ions from aqueous solution is a promising field of research, which has a great scope of further study. Developing materials with a specific texture and modifying the surface chemistry to increase the adsorption capacity are some issues for implementation in these materials.

The chemical vapor deposition is an excellent method to obtain Ti-SBA-15-h with a high disperse titanium on the SBA-15 surface. The $TiO_2$ is very important in photocatalytic process. Actually, different researches are putting efforts to obtain mesoporous materials with titanium to increase the yield in different reactions like photodegradation of organic compounds in water. This is an approximation to understand the synthesis of SBA-15, its mechanisms, and the way to include hetero-elements by chemical vapor deposition. It is necessary to further this

line of research with the aim to synthesize photocatalysts that are efficient, cheap, and reusable for the benefit of the environment.

## Acknowledgements

The authors thank the University of the Andes (Bogota, Colombia) and National University of Colombia (Bogotá) by the framework agreement between the two institutions under which this research was developed. Special thanks to the Faculty of Science and the Vice-Rectory of Research at the University of the Andes (Bogota, Colombia) for funding this research and the "Semilla Project" 2016-1 of Faculty of Sciences, University of the Andes (Bogota, Colombia).

## Author details

Rafael Alberto Fonseca-Correa[1], Yesid Sneider Murillo-Acevedo[1], Liliana Giraldo-Gutiérrez[2] and Juan Carlos Moreno-Piraján[1*]

*Address all correspondence to: jumoreno@uniandes.edu.co

1 Department of Chemistry, Research Group Porous Solids and Calorimetry, Faculty of Sciences, University of the Andes, Bogotá, Colombia

2 Department of Chemistry, Faculty of Sciences, National University of Colombia, Bogotá, Colombia

## References

[1] Zulamita Z.B., Carrasco M.F., Vicente J., Moreno C.C. Langmuir. 2013; 29: 6166–6173.

[2] Yong K., Ya Z., Xiaodeng S., Sheng C., Mong Y., Kaiming T., Junjun Z. Journal of Non-Crystalline Solids. 2012; 358: 3150–3155.

[3] Geng P.W., Junbing Y., Dapeng W., Rui X., Khalil A., Chung X.L. Materials Letters. 2014; 115: 1–4.

[4] Jie Z., Rang L., Weiling N., Yanjun W., Xinglung G. International Journal of Hydrogen Energy. 2013; 38: 10864–10870.

[5] Zapata B.Z., Moreno C.C., Carrasco M.F. Journal of Sol-Gel Science and Technology. 2015; 75 (2): 407–412.

[6] Pierre A.C., Pajonk G.M. Chemical Reviews. 2002; 102: 4243–4265.

[7] Pekala, R.W. US4873218 (1989).

[8] Pekala, R.W. US4997804 (1991).

[9] Niaping L., Jun S., Dong L. Microporous and Mesoporous Materials. 2013; 167: 176–181.

[10] Moreno C.C., Maldonado H.F.J. Carbon. 2005; 43: 455–465.

[11] Brinker C.J., Scherer G.W. Sol-Gel Science: The Physics and Chemistry of Sol-Gel Processing. Academic Press: San Diego, CA, USA, 1990.

[12] Ai D., Bin Z., Zhihua Z., Jun S. Materials. 2013; 6: 941–968.

[13] Yousheng T., Morinobu E., Katsumi K. Recent Patents on Chemical Engineering. 2008; 1 (3): 192–200.

[14] Alain C.P., Gérard M.P. Chemical Reviews. 2002; 102 (11): 4243–4265.

[15] Boehm H.P. Carbon. 2002; 40: 145–149.

[16] Laoufi N.A., Tassalit D., Bentahar F. Global Nest Journal. 2008; 10: 404–418.

[17] Kumar R.P., Venkata L.R.P., Kwon E., Ki H.K., Tahmina A., Sudhakar K. Environment International. 2016; 91: 94–103.

[18] Hou Y., Qiujun L., Wang H., Haitao L., Youyu Z., Shiying Z. Materials Letters. 2016; 173: 13–17.

[19] Linsebigler A., Lu G., Yates J.T. Chemical Reviews. 1995; 95: 735–758.

[20] Fujishima A., Rao N.T., Rryk D.A. Journal of Photochemistry and Photobiology C: Photochemistry Reviews. 2000; 1: 1.

[21] Lin X H., Wu Y., Xiang J., He D., Li S.F.Y, App. Catal B: Environ. 2016; 74, 64–74.

[22] Prieto R.L., Oller I., Klamerth N., Agüera A., Rodríguez E.M., Malato S. Water Research. 2013; 47: 1521–1528.

[23] Nan C.M., Jin B., Chow C.W.K., Saint C. Water Research. 2010; 44: 2997–3027.

[24] Impéror C.M., Davidson P., Davidson A. Journal of the American Chemical Society. 2000; 122:11925–11933.

[25] Flodstrom K., Alfredson V. Microporous and Mesoporous Materials. 2003; 59: 167–176.

[26] Brinker C.J. Journal of Non-Crystalline Solids. 1988; 100: 31–50.

[27] Hench L.L., West J.K. Chemical Reviews. 1990; 90: 33–72.

[28] Meynen V., Cool P., Vasant E.F. Microporous and Mesoporous Materials. 2007; 104: 26–38.

[29] Corma A. Chemical Reviews. 1997; 97: 2373–2419.

[30] Kresge C.T., Leonowicz M.E., Roth W.J., Vartuli J.C., Beck, J.S. Nature. 1992; 359: 710–712.

[31] Segura Y., Meynen V., Van der Voort P., Mees F., Vasant E.F. Journal of Physical Chemistry B. 2004; 108: 3794–3800.

[32] Chen Y.Y., Huang Y.L., Xiu J.H., Han X.W., Bao X.H. Applied Catalysis A: General. 2004; 273: 185–191.

[33] Kinney J., Staley R. Journal of Physical Chemistry. 1983; 87: 3735–3740.

[34] Junming Y., Wangcheng Z., Xiaohui L., Yanglong G., Yanqin W., Yun G., Guanzhong L. Microporous and Mesoporous Materials. 2012; 148: 131–136.

[35] Oguraa M., Guillet N.R., Brouri D., Casale S., Blanchard J., Cychosz K., Thommes M., Thomas C. Microporous and Mesoporous Materials. 2016; 225: 440–449.